THE SMALL-SCALE DYNAMO AND NON-IDEAL MAGNETOHYDRODYNAMICS IN PRIMORDIAL STAR FORMATION

JENNIFER SCHOBER[1], DOMINIK SCHLEICHER[2], CHRISTOPH FEDERRATH[1,3], SIMON GLOVER[1],
RALF S. KLESSEN[1], AND ROBI BANERJEE[4]

[1] Zentrum für Astronomie der Universität Heidelberg, Institut für Theoretische Astrophysik, Albert-Ueberle-Str. 2, D-69120 Heidelberg, Germany;
schober@stud.uni-heidelberg.de, christoph.federrath@monash.edu, glover@uni-heidelberg.de, klessen@uni-heidelberg.de
[2] Institut für Astrophysik, Georg-August-Universität Göttingen, Friedrich-Hund-Platz 1, D-37077 Göttingen, Germany; dschleic@astro.physik.uni-goettingen.de
[3] Monash Centre for Astrophysics (MoCA), School of Mathematical Sciences, Monash University, Vic 3800, Australia
[4] Hamburger Sternwarte, Gojenbergsweg 112, D-21029 Hamburg, Germany; banerjee@hs.uni-hamburg.de

ABSTRACT

We study the amplification of magnetic fields during the formation of primordial halos. The turbulence generated by gravitational infall motions during the formation of the first stars and galaxies can amplify magnetic fields very efficiently and on short timescales up to dynamically significant values. Using the Kazantsev theory, which describes the so-called small-scale dynamo—a magnetohydrodynamical process converting kinetic energy from turbulence into magnetic energy—we can then calculate the growth rate of the small-scale magnetic field. Our calculations are based on a detailed chemical network and we include non-ideal magnetohydrodynamical effects such as ambipolar diffusion and Ohmic dissipation. We follow the evolution of the magnetic field up to larger scales until saturation occurs on the Jeans scale. Assuming a weak magnetic seed field generated by the Biermann battery process, both Burgers and Kolmogorov turbulence lead to saturation within a rather small density range. Such fields are likely to become relevant after the formation of a protostellar disk and, thus, could influence the formation of the first stars and galaxies in the universe.

1. INTRODUCTION

Magnetic fields play an important role in star formation. There is increasing evidence that dynamically important magnetic fields were also present in the early universe (Banerjee & Jedamzik 2004; Silk & Langer 2006; Schleicher et al. 2010; Sur et al. 2010; Federrath et al. 2011a; Turk et al. 2012). If this turns out to be true, current models for the formation of the first stars and galaxies need to be revisited.

The theory of primordial star formation has gone through a change recently. It was previously assumed that the first stars were extremely massive and isolated (Abel et al. 2002; Bromm & Larson 2004). However, new high-resolution calculations (Stacy et al. 2010; Clark et al. 2011; Smith et al. 2011; Greif et al. 2011, 2012) show that the accretion disk of a collapsing primordial halo fragments into multiple stars. The inclusion of magnetic fields could change this picture again. The magnetic pressure can stabilize an accretion disk and, depending on the field strength, suppress the fragmentation (Machida et al. 2004; Hennebelle & Teyssier 2007; Price & Bate 2007; Peters et al. 2011; Seifried et al. 2011). So far, there are only a few studies of primordial star formation that include magnetic fields (Tan & Blackman 2004; Maki & Susa 2004, 2007; Silk & Langer 2006; Schleicher et al. 2010; Machida 2010; Federrath et al. 2011b; Sur et al. 2012; Turk et al. 2012). The magnetic field is expected to have similar effects to those seen in present-day star formation, such as the launching of winds and jets (Machida et al. 2006, 2008a). The latter eject gas from the accretion disk which could otherwise have collapsed onto the star. Thus, the star formation efficiency is reduced, especially for high-mass stars (Tan & Blackman 2004; Machida 2010). Strong jets can transport matter even out of the star-forming halo, leading to a magnetization of the intergalactic medium (Xu et al. 2011).

To develop primordial star formation theory further, we need to know the structure and strength of the magnetic fields. The mechanism we suggest for producing strong fields is the small-scale dynamo. This magnetohydrodynamical (MHD) process amplifies weak magnetic seed fields exponentially by converting kinetic energy from the turbulence into magnetic energy.

Kazantsev (1968) developed a theory for describing the small-scale or turbulent dynamo. The main equation of this theory is the Kazantsev equation, the eigenvalue of which is the growth rate of the magnetic energy. There are different solutions of this equation (Rogachevskii & Kleeorin 1997; Kleeorin & Rogachevskii 2011; Schekochihin et al. 2002a). In this work, we use the solution proposed by Schober et al. (2012), which takes into account different types of turbulence. The growth rates of the magnetic field obtained in that work are comparable to previous results for Kolmogorov turbulence (Subramanian 1997; Brandenburg & Subramanian 2005).

We model the physical and chemical processes during the collapse of a primordial halo to quantitatively determine the properties of the small-scale dynamo. We calculate the magnetic Prandtl number and the magnetic Reynolds number. The latter is compared to the critical magnetic Reynolds number for small-scale dynamo action. Furthermore, we calculate the growth rate, which depends on the magnetic Prandtl number and the hydrodynamic Reynolds number. We assume a weak initial magnetic field of 10^{-20} G on the viscous scale produced by the Biermann battery (Biermann 1950; Kulsrud et al. 1997; Xu et al. 2008). This allows us to determine the evolution of the magnetic field strength during the collapse.

The structure of our study is as follows. In Section 2, we review the properties of primordial gas. We present our numerical calculation of the chemistry and thermal evolution of the gas and discuss the characteristic magnetohydrodynamical
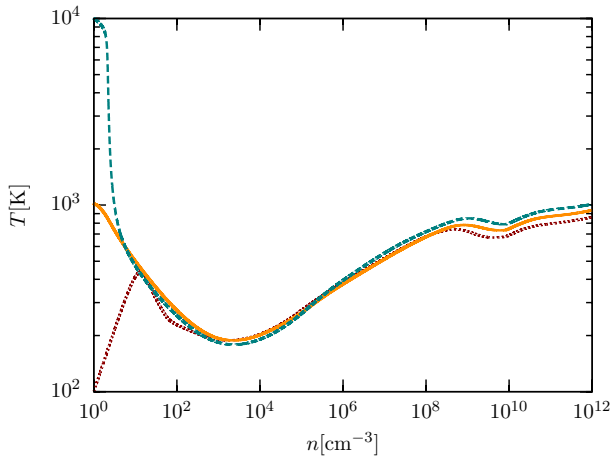
Figure 1. Temperature as a function of the number density. The different lines indicate different initial conditions. The dashed green line corresponds to an initial temperature of 10^4 K, the dotted red line to 10^3 K, and the solid orange line to 10^2 K.

(A color version of this figure is available in the online journal.)

Figure 2. Fractional abundances of different chemical species as a function of the number density.

(A color version of this figure is available in the online journal.)

quantities. Furthermore, we discuss the origin of turbulence and weak magnetic seed fields in primordial halos, which are essential for operation of the small-scale dynamo. Section 3 concentrates on the small-scale magnetic field evolution. We give the basic equations of the Kazantsev theory and the resulting growth rates of the magnetic energy. We apply these results for the small-scale magnetic field to our model for the collapse of a primordial halo. In Section 4, we present a model for the transport of the magnetic energy to larger scales. This allows us to calculate the magnetic energy on the Jeans scale of the primordial halo.

2. PROPERTIES OF THE PRIMORDIAL GAS

2.1. Chemical and Thermal Evolution

We determine the chemical and thermal evolution of gravitationally collapsing primordial gas using the one-zone model of Glover & Savin (2009), together with a modification implemented by Schleicher et al. (2009) that relates the collapse time to the equation of state. Moreover, we have included additional Li$^+$ chemistry by using the reaction rates from Bovino et al. (2011b) and HeH$^+$ chemistry according to Bovino et al. (2011a). Glover & Savin (2009) model the chemistry of the gas with a chemical network that includes around 30 different atomic and molecular species linked by around 400 different chemical reactions. In our calculations, we use the same initial chemical abundances as in the default model in Glover & Savin (2009). The elemental abundances of helium, deuterium, and lithium relative to hydrogen are taken to be 0.083 for helium, 2.6×10^{-5} for deuterium, and 4.3×10^{-10} for lithium (Cyburt 2004). The initial density and temperature of the gas were assumed to be $n_0 = 1$ cm^{-3} and $T_0 = 1000$ K, respectively, but we have verified that our results are not sensitive to these values.

In the one-zone model the mass density ρ evolves as

$$\frac{d\rho}{dt} \propto \frac{\rho}{t_{\rm ff}}, \qquad (1)$$

where $t_{\rm ff} = \sqrt{3\pi/(32G\rho)}$ is the free-fall time. Moreover, the temperature evolution is determined by the energy equation,

$$\frac{d\epsilon}{dt} = \frac{p}{\rho^2}\frac{d\rho}{dt} - \Lambda_{\rm cool} + \Lambda_{\rm heat}, \qquad (2)$$
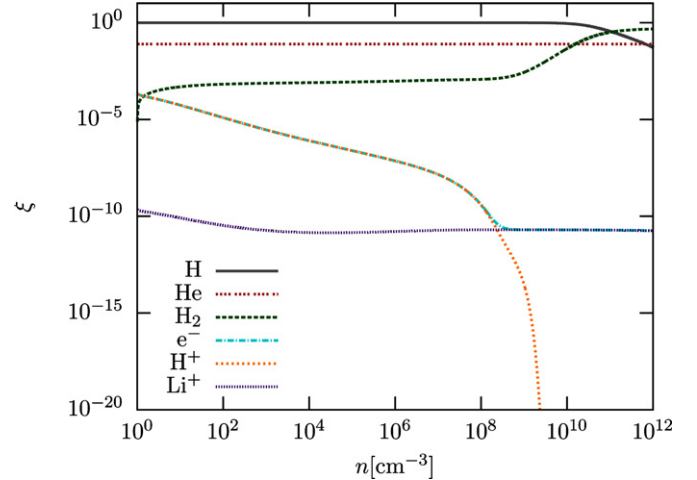
where ϵ is the specific internal energy, p is the thermal pressure, and $\Lambda_{\rm cool}$ and $\Lambda_{\rm heat}$ are the total cooling and heating rates per unit mass, respectively. The resulting temperature evolution is shown in Figure 1. Besides the initial temperature of 10^3 K, we also show in this figure the results for initial temperatures of 10^2 K and 10^4 K. Our calculations result in roughly the same evolution for all the initial temperatures after an increase in the density of about one order of magnitude.

In Figure 2, the fractional abundances of H, He, H$_2$, H$^+$, Li$^+$, and free electrons vary with increasing density in our calculations. The abundance of H is constant at low densities, but decreases at densities higher than about 10^{10}cm^{-3} due to the formation of H$_2$. As there is no dust in primordial gas, large quantities of H$_2$ are produced only at high densities, via the three-body reactions:

$$H + H + H \rightarrow H_2 + H, \qquad (3a)$$

$$H + H + He \rightarrow H_2 + He, \qquad (3b)$$

$$H + H + H_2 \rightarrow H_2 + H_2. \qquad (3c)$$
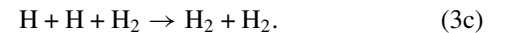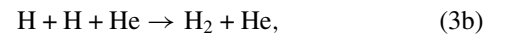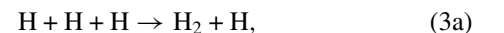
For the magnetic properties of the primordial gas the abundances of the charged species are especially important. They determine for example the conductivity, which is calculated in the next section. At densities $n < 10^8$ cm^{-3}, ionized hydrogen is the main positive ion, while at higher densities, Li$^+$ dominates. The sharp drop in the H$^+$ abundance at densities $n > 10^8$ cm^{-3} results from the removal of H$^+$ from the gas by the reaction chain (Glover & Savin 2009)

$$H_2 + H^+ \rightarrow H_3^+ + \gamma, \qquad (4a)$$

$$H_3^+ + e^- \rightarrow H_2 + H. \qquad (4b)$$
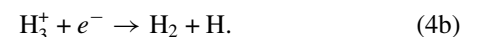
2.2. Characteristic Magnetohydrodynamical Quantities

Viscosity. It can be shown that the kinematic viscosity is

$$\nu = \frac{1}{4d^2n}\left(\frac{kT}{\pi m}\right)^{1/2}, \qquad (5)$$

if the molecules are assumed to be rigid spheres (Choudhuri 1998). Here, $n = \rho/m$ is the number density, k is the Boltzmann constant, and T is the temperature. Furthermore, $d = \sum_i \xi_i d_i$ is the mean particle diameter and $m = \sum_i \xi_i m_i$ the mean mass. ξ_i is the relative abundance of the species i, and m_i and d_i are the masses and the van der Waals diameters, respectively. The temperature as well as the abundances of the individual species are functions of the number density.

Diffusivity. For calculating the magnetic diffusivity η we need the conductivity of the gas. In a plasma the three most important contributions to the conductivity of a neutral species (indicated by index n) are (Wardle & Ng 1999)

$$\sigma_{||,n} = \frac{c}{B} \sum_s \xi_s n q_s \beta_{ns}, \qquad (6a)$$

$$\sigma_{P,n} = \frac{c}{B} \sum_s \xi_s n q_s \frac{\beta_{ns}}{1 + \beta_{ns}^2}, \qquad (6b)$$

$$\sigma_{H,n} = \frac{c}{B} \sum_s \xi_s n q_s \frac{1}{1 + \beta_{ns}^2}, \qquad (6c)$$

as given in Pinto et al. (2008). The Hall parameters β_{ns} are defined as

$$\beta_{ns} = \frac{q_s B}{m_s c} \frac{m_s + m_n}{m_n \xi_n n \langle \sigma v \rangle_{sn}}. \qquad (7)$$

Here, m_n and m_s are the masses of the neutral and the charged particles, ξ_n and ξ_s are the abundance fractions of the species, and $\langle \sigma v \rangle_{sn}$ is the momentum transfer rate coefficient. We take these coefficients, which are functions of the temperature, from Pinto & Galli (2008), where we use the polarization approximation for Li$^+$.

The two dominant effects that lead to the dissipation of magnetic energy are the Ohmic resistivity and ambipolar diffusion. We can neglect the contribution of the Hall effect to the resistivity, as here the force acts perpendicular to the current and, thus, no energy is dissipated into heat. We calculate the distributions of the Ohmic resistivity and the ambipolar diffusion by

$$\eta_{Ohm,n} = \frac{c^2}{4\pi \sigma_{||,n}}, \qquad (8a)$$

$$\eta_{AD,n} = \frac{c^2}{4\pi} \left(\frac{\sigma_{P,n}}{\sigma_{P,n}^2 + \sigma_{H,n}^2} - \frac{1}{\sigma_{||,n}} \right). \qquad (8b)$$

We focus on the most important neutral species H, He, and H$_2$ and the charged species H$^+$, e^-, and Li$^+$. For each neutral species we calculate the resistivities $\eta_{Ohm,n}$ and $\eta_{AD,n}$. The magnetic field strength B drops out in the Ohmic case. Finally, the total Ohmic magnetic diffusivity is $\eta_{Ohm} = \sum_n \eta_{Ohm,n}$ and the total resistivity due to ambipolar diffusion is $\eta_{AD} = 1/(\sum_n \eta_{AD,n}^{-1})$.[5]

Reynolds numbers. The hydrodynamic and magnetic Reynolds numbers are defined as

$$Re \equiv \frac{VL}{\nu} \qquad (9a)$$

$$Rm \equiv \frac{VL}{\eta}, \qquad (9b)$$

---
[5] From private communication with Daniele Galli.
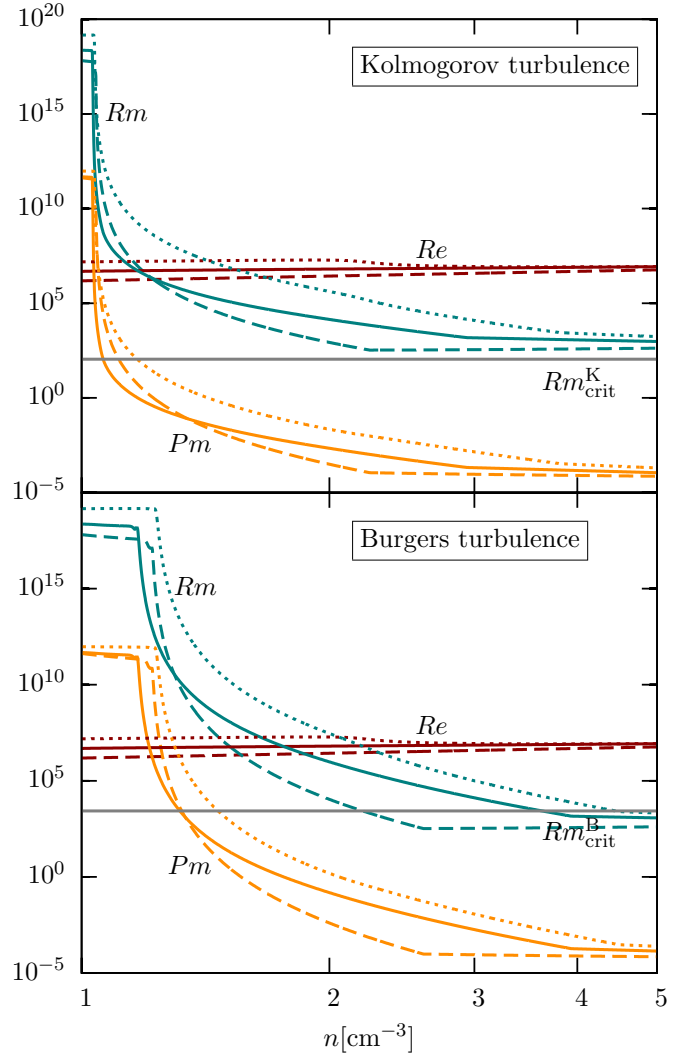
Figure 3. Hydrodynamic and magnetic Reynolds numbers, Re and Rm, as well as the magnetic Prandtl numbers, Pm, on the current Jeans scale. The numbers are presented as a function of the hydrogen nuclei number density, n. The solid lines represent an initial temperature of 10^3 K, the dashed lines 10^2 K, and the dotted lines 10^4 K. Moreover, the horizontal lines indicate the critical magnetic Reynolds number for Kolmogorov and Burgers turbulence ($Rm_{crit}^K = 107$ and $Rm_{crit}^B = 2718$) as derived in Schober et al. (2012). The rapid decrease of Rm and Pm from the very high starting values is caused by the exponential dynamo amplification of the magnetic field. We show the results for Kolmogorov turbulence in the upper plot and the results for Burgers turbulence in the lower plot.

(A color version of this figure is available in the online journal.)

where L is the length of the largest turbulent fluctuations and V is the typical velocity on that scale. Note that we give these numbers on the forcing scale, i.e., the Jeans scale, which means $L = \ell_J$ and $V = v_J$.

For the calculation of the magnetic Reynolds number we use the sum of η_{Ohm} and η_{AD}. The resulting Reynolds numbers are shown in Figure 3 as a function of the density. The critical magnetic Reynolds numbers (15) are also indicated for the two extreme types of turbulence.

Magnetic Prandtl number. The definition of the magnetic Prandtl number is

$$Pm \equiv \frac{Rm}{Re} = \frac{\nu}{\eta}. \qquad (10)$$

We can calculate this quantity by using Equations (5) and (8). In Figure 3, the density dependency of the magnetic Prandtl

number is shown for both Kolmogorov and Burgers turbulence. For clarification we point out that the rapid decrease of the magnetic Reynolds and Prandtl numbers is caused by the dynamo amplification of the magnetic field. At the beginning of the collapse Ohmic resistivity is the dominant diffusion process. With increasing magnetic field η_{AD} increases proportional to B^2 (see Equations (6)–(8)) and becomes the main process for magnetic diffusion. Since Rm and Pm are both proportional to $1/\eta_{AD}$, in the limit where $\eta_{AD} \gg \eta_{Ohm}$, both decrease rapidly with increasing magnetic field strength.

In addition, we tested the influence of varying the initial temperature on the evolution of the Reynolds numbers and the magnetic Prandtl number. For the initial temperature ranging from 10^2 K to 10^4 K we found only small variations in the Reynolds numbers and the magnetic Prandtl number, as illustrated in Figure 3.

2.3. Turbulence

Turbulence is an omnipresent phenomenon in astrophysics. Turbulence is observed, for example, in the convection zone of stars, in accretion disks, and in the interstellar medium.

For the first star-forming halos considered here, we assume that turbulence is driven by virialization (Wise & Abel 2007; Greif et al. 2008) or by accretion of gas into the center of the halos (Klessen & Hennebelle 2010; Elmegreen & Burkert 2010; Federrath et al. 2011b). The presence of turbulence affects star formation strongly, as the turbulent pressure works against the collapse to a star (Vazquez-Semadeni et al. 1998; Mac Low & Klessen 2004; Krumholz & McKee 2005; McKee & Ostriker 2007). Moreover, Federrath et al. (2011b) show in a Fourier analysis that the turbulence is effectively driven on the Jeans scale.

There are different types of turbulence. In this paper we concentrate on the two extreme cases, Kolmogorov turbulence and highly compressible Burgers turbulence. The different types are described in the inertial range by the relation between the length scale ℓ and the velocity v on that scale,

$$v \propto \ell^{\vartheta}. \qquad (11)$$

The exponent ϑ ranges from 1/3 for incompressible turbulence (Kolmogorov 1941) to 1/2 for highly compressible turbulence (Burgers 1948). In real astrophysical objects, we expect the turbulence index ϑ to lie between these extreme cases (Kritsuk et al. 2007; Schmidt et al. 2008; Federrath et al. 2010).

2.4. Magnetic Seed Fields

There are different theories that describe the origin of weak primordial magnetic fields. The first seed fields could already have been produced during inflation. Turner & Widrow (1988) find that a magnetic field $B_0 \approx 10^{-25}$ to 10^{-1} nG on a scale of 1 Mpc can be produced when the conformal invariance is broken.

Following Sigl et al. (1997), there is also a possibility to create a magnetic field during first-order phase transitions in the very early universe. They predict a field strength $B_0 \approx 10^{-20}$ nG from the electroweak phase transition and $B_0 \approx 10^{-11}$ nG from the QCD phase transition on a scale of 10 Mpc.

Battery mechanisms are another popular way to generate magnetic fields. The so-called Biermann battery uses the fact that electrons and ions have very different masses. If there is a pressure gradient in the plasma the particles get accelerated. Due to their smaller masses the electrons are more strongly

accelerated than the ions. This leads to charge separation and an electric field is generated. If the electron density n_e is constant in space the electric field is static; however, if it varies in space electric currents are generated, which give rise to a corresponding magnetic field. Note that for the Biermann term to be non-zero the cross-product of the electron pressure gradient and the electron density gradient needs to be non-zero (Biermann 1950; Kulsrud & Zweibel 2008).

3. MAGNETIC FIELD AMPLIFICATION ON THE VISCOUS SCALE

In this section, we analyze the evolution of the small-scale magnetic field. We outline the Kazantsev theory, which gives the growth rates of the magnetic field on the viscous scale. Together with the amplification due to gravitational compression and dissipation processes we can calculate the resulting small-scale magnetic field evolution.

3.1. Small-scale Dynamo Growth

Kazantsev theory. An arbitrary magnetic field **B** can, in general, be separated into a mean component $\mathbf{B}_0$ and a fluctuating component $\delta\mathbf{B}$ with

$$\mathbf{B} = \mathbf{B}_0 + \delta\mathbf{B}. \qquad (12)$$

The induction equation,

$$\frac{\partial \mathbf{B}}{\partial t} = \nabla \times (\mathbf{v} \times \mathbf{B} - \eta \nabla \times \mathbf{B}), \qquad (13)$$

describes the time evolution of this field, where **v** is the velocity and η is the magnetic diffusivity. Substitution of Equation (12) into the induction equation leads to two equations: an equation for the large-scale field evolution and the Kazantsev equation (Kazantsev 1968; Brandenburg & Subramanian 2005), which describes the small-scale evolution of the field.

The derivation of the Kazantsev equation is based on the assumption that the fluctuations of the magnetic field as well as the fluctuations of the velocity field are homogeneous and isotropic even if the mean fields are not isotropic. Furthermore, the fluctuations are assumed to be a Gaussian random field with zero mean and the velocity fluctuations are assumed to be delta-correlated in time. For simplicity the helicity of the magnetic field is neglected. With these assumptions the Kazantsev equation is

$$-\kappa_{\text{diff}}(r)\frac{d^2\psi(r)}{d^2r} + U(r)\psi(r) = -\Gamma\psi(r). \qquad (14)$$

The eigenfunctions of this equation are related to the longitudinal correlation function of the magnetic fluctuations $M_L(r, t)$ by $M_L \equiv 1/(r^2\sqrt{\kappa_{\text{diff}}})\psi(r)\exp(2\Gamma t)$. We call Γ the growth rate of the small-scale magnetic field. The function κ_{diff} is the magnetic diffusion coefficient, which contains in addition to the magnetic diffusivity η a scale-dependent turbulent diffusivity also. U is called the "potential" of the Kazantsev equation. Both κ_{diff} and U depend only on the correlation function of the turbulent velocity field and the magnetic diffusivity. The correlation function of the turbulent velocity field in turn depends on the different types of turbulence.

With a model for the turbulent correlation function, Schober et al. (2012) solved the Kazantsev equation (Equation (14)) with the WKB approximation. They found that the critical

magnetic Reynolds number for dynamo action Rm_{crit} increases with compressibility. The values that Rm needs to exceed are

$$Rm_{crit}^K \approx 107, \qquad (15a)$$

$$Rm_{crit}^B \approx 2718, \qquad (15b)$$

for Kolmogorov and Burgers turbulence, respectively.

Moreover, Schober et al. (2012) found different growth rates of the magnetic field for different turbulence models, with

$$\Gamma = \frac{(163 - 304\vartheta)}{60} \frac{V}{L} Re^{(1-\vartheta)/(1+\vartheta)} \qquad (16)$$

in the limit of infinite magnetic Prandtl numbers. Here V is the typical velocity on the largest scale of the turbulent eddies of size L and Re is the hydrodynamical Reynolds number.

In this paper, we analyze the two extreme types of turbulence, Kolmogorov with $\vartheta = 1/3$ and Burgers with $\vartheta = 1/2$. We find in the limit of large magnetic Prandtl numbers

$$\Gamma^K = \frac{37}{36} \frac{V}{L} Re^{1/2}, \qquad (17a)$$

$$\Gamma^B = \frac{11}{60} \frac{V}{L} Re^{1/3}. \qquad (17b)$$

For the typical velocity of the largest fluctuations we use the sound speed $V = v_J \approx \sqrt{\gamma kT/m}$, as the Mach number in the first star-forming halos is roughly one (Greif et al. 2008). Here γ is the adiabatic index. We take L to be the Jeans length, as this is the effective driving scale for turbulence in a collapsing system (Schleicher et al. 2010; Federrath et al. 2011b). Hence we set $L \approx \ell_J = \sqrt{\gamma kT/(Gm^2 n)}$, where G is the gravitational constant.

We compare the growth rate of the small-scale dynamo Γ on the viscous scale $\ell_\nu = l_J Re^{-1/(1+\vartheta)}$ to the inverse free-fall time $1/t_{ff} = [3\pi/(32Gmn)]^{-1/2}$. The result is shown in Figure 4. In our model, the magnetic field on the fastest growing scale increases one to three orders of magnitude faster than the halo collapses. Note that the dynamo growth is exponential in time.

Gravitational compression. The gravitational compression due to the collapse of the halo provides additional amplification of the magnetic field. As long as the condition of flux freezing is fulfilled, the magnetic field B increases with density like

$$B \propto n^{2/3} \qquad (18)$$

for spherically symmetric collapse. Before the dynamo saturates, the amplification by gravitational compression is minor compared to the dynamo growth.

Dissipation. Part of the magnetic energy is converted into heat by dissipation processes. The dissipation term in the induction Equation (13) is $\eta \nabla^2 \mathbf{B}$. We consider Ohmic dissipation and ambipolar diffusion and approximate this by $\eta B/\ell^2$ and $\partial B/\partial t$ by $B\Gamma_{Ohm}$ and $B\Gamma_{AD}$, respectively. We get

$$\Gamma_{Ohm} \approx \frac{\eta_{Ohm}}{\ell^2}, \qquad (19a)$$

$$\Gamma_{AD} \approx \frac{\eta_{AD}}{\ell^2}. \qquad (19b)$$

Γ_{Ohm} and Γ_{AD} are the rates of magnetic energy dissipation by Ohmic resistivity and ambipolar diffusion.
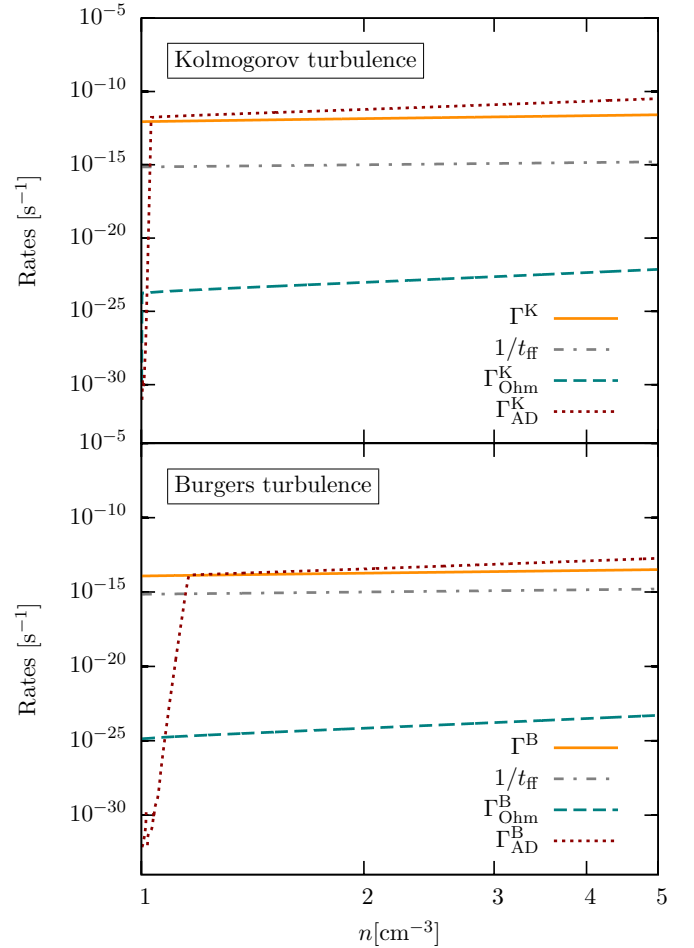
Figure 4. Different characteristic rates on the viscous scale as a function of the density. We compare the growth rate of the magnetic field (solid orange line) to the inverse free-fall time (dash-dotted gray line) and the dissipation rates (Ohmic dissipation: dashed green line, ambipolar diffusion: dotted red line). We show the results for Kolmogorov turbulence in the upper plot and the results for Burgers turbulence in the lower plot.

(A color version of this figure is available in the online journal.)

3.2. Critical Magnetic Reynolds Number

The dependency of the magnetic Reynolds number Rm on the number density is shown in Figure 3 for the two extreme types of turbulence. We also indicate the critical magnetic Reynolds number for small-scale dynamo action Rm_{crit}. One can see that the magnetic Reynolds number is larger than Rm_{crit} at the onset of the collapse. For densities above roughly $4 \, cm^{-3}$ Rm becomes smaller than the critical value in the case of Burgers turbulence. For Kolmogorov turbulence Rm also becomes smaller than Rm_{crit} for high densities, which are not shown in Figure 3. However, as we see below, at this point the dynamo is already saturated on the small scale as well as on the large scale. Thus, in the density regime where the small-scale dynamo operates, the condition $Rm > Rm_{crit}$ is always fulfilled.

3.3. Resulting Small-scale Magnetic Field

In principle, the magnetic energy density, $E_B = B^2/(8\pi)$, evolves as

$$\frac{dE_B}{dt} = \left[\Gamma + \frac{4}{3n} \frac{dn}{dt} - \Gamma_{Ohm} - \Gamma_{AD}(E_B) \right] E_B, \qquad (20)$$

where we assume spherically symmetric collapse.

By solving Equation (20) numerically we find the evolution of the magnetic energy density on small scales. In Figure 7, we show the resulting growth of the magnetic field strength. As an initial field strength B_0 we use 10^{-20} G on the viscous scale, which is a conservative value for a field generated by a Biermann battery (Biermann 1950; Xu et al. 2008). The field strength grows extremely rapidly as the density increases. However, we cannot trust the whole evolution of the magnetic field exactly as shown in Figure 7. When the field has become strong enough, the magnetic Prandtl number becomes unity or less (see Figure 3). Then the WKB approximation breaks down and Equations (17) are no longer valid. Complementary studies have shown, however, that the small-scale dynamo still operates for Pm < 1 (Boldyrev & Cattaneo 2004; Schekochihin et al. 2005, 2007; Eyink 2011), although the growth rate may decrease by a factor of a few. We note that Boldyrev & Cattaneo (2004) find in their studies that the critical magnetic Reynolds number increases with decreasing magnetic Prandtl number. Furthermore, we see in Figure 4 that the ambipolar diffusion rate becomes higher than the growth rate of the magnetic field. In this regime, Equation (16) is no longer a solution of Equation (14). We expect that the field grows at the rate given by Equation (16) almost until saturation, then decreases and the field reaches saturation more slowly.

3.4. Validity of our Approximation

In Figure 3, the magnetic Prandtl number Pm is shown as a function of the density. Pm starts with an extremely high value of roughly 10^{12} and then after a rather constant phase decreases rapidly. The magnetic Prandtl number is defined in Equation (10) with $\eta = \eta_{\text{Ohm}} + \eta_{\text{AD}}$. For low densities the Ohmic resistivity, which is independent of the magnetic field strength dominates. With increasing density the magnetic field increases due to the dynamo amplification and with $\eta_{\text{AD}} \propto B^2$ the ambipolar diffusion rate becomes dominant. In this regime the magnetic Prandtl number decreases proportional to B^{-2}. As the magnetic field increases exponentially during the small-scale dynamo amplification at the beginning of the collapse, the magnetic Prandtl number decreases rapidly.

The approximation of large magnetic Prandtl numbers (Schober et al. 2012) is accurate during most of the dynamo growth. At the end of the dynamo phase, however, Pm reaches unity, decreases even further and our approximations eventually break down. Schober et al. (2012) show that for decreasing Pm the growth rate decreases. However, they make no prediction for the regime Pm $\approx$ 1. But numerical simulations show that the dynamo also operates in this regime (e.g., Federrath et al. 2011b). For Pm $\ll$ 1 there is again analytical evidence for small-scale dynamo action (e.g., Schekochihin et al. 2007). We note that this treatment concerns the viscous scale only.

4. MAGNETIC FIELD AMPLIFICATION ON LARGER SCALES

4.1. Model for the Transport of Magnetic Energy to Larger Scales

After the magnetic field saturates on the viscous scale the peak of the magnetic energy spectrum moves to larger scales. In this section we present a model for the time evolution of the magnetic energy spectrum. The situation is illustrated schematically in Figure 5. Here we indicate three different curves, which represent different times. The dashed green line is the spectrum at the time of saturation on the viscous scale,
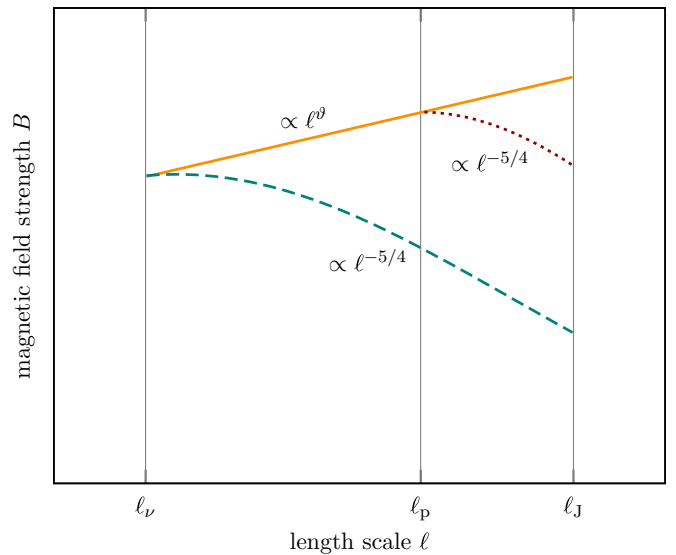
Figure 5. Schematic model for the time evolution of the spectrum of the magnetic field strength in the inertial range of turbulence. For simplicity we use a fixed frame of reference, where the viscous and the Jeans scales stay constant. The different colors and line types represent the spectrum at different times. The green dashed line shows the spectrum at saturation on the viscous scale. To larger scales the spectrum decreases according to the Kazantsev slope ($B \propto \ell^{-5/4}$). At a time after saturation on the viscous scale the spectrum is indicated by the dotted red line. Finally, the solid orange line shows the spectrum when the field is saturated on the Jeans scale.

(A color version of this figure is available in the online journal.)

the dotted red line shows a later time and the solid orange line represents an even later point in time at which the magnetic field has saturated on the Jeans scale.

During saturation, the coherence length of the magnetic field shifts toward larger scales, a well-known behavior for the small-scale dynamo (Schekochihin et al. 2002b; Brandenburg & Subramanian 2005), recently shown to be true also in a collapsing system (Sur et al. 2012). Analytical arguments suggest that this occurs on the eddy timescale of the current peak scale ℓ_{p},

$$\frac{\ell_{\text{p}}}{v_{\text{p}}} = \frac{\ell_{\text{J}}}{v_{\text{J}}} \left(\frac{\ell_{\text{p}}}{\ell_{\text{J}}} \right)^{1-\vartheta}, \tag{21}$$

where we used $v_{\text{p}} = v_{\text{J}}(\ell_{\text{p}}/\ell_{\text{J}})^{\vartheta}$. Considering that the peak scale moves from the viscous scale $\ell_\nu(t_\nu)$ toward larger scales, we find for the time dependency of the peak scale

$$\ell_{\text{p}}(t) = \ell_\nu(t_\nu) + \left(\frac{v_{\text{J}}}{\ell_{\text{J}}^{\vartheta}}(t - t_\nu) \right)^{1/(1-\vartheta)}, \tag{22}$$

where t_ν is the point in time when saturation occurs on the viscous scale.

The slope of the curves proportional to $\ell^{-5/4}$ is known as the Kazantsev slope in real space,[6] which can be derived from the Fourier-transformed Kazantsev equation (Equation (14)) (Brandenburg & Subramanian 2005). This characteristic slope is also observed in simulations (Federrath et al. 2011b; Xu et al. 2011). The curve that connects the peak maxima at different

---

[6] In many references, the magnetic energy spectrum is given as a function of the wave number k, defined for example as $B^2/(8\pi\rho) = 1/2 \int M(k)dk$. In this case the Kazantsev slope is $M(k) \propto k^{3/2}$. From this we find $B^2 \propto k^{5/2}$ and $B \propto \ell^{-5/4}$.
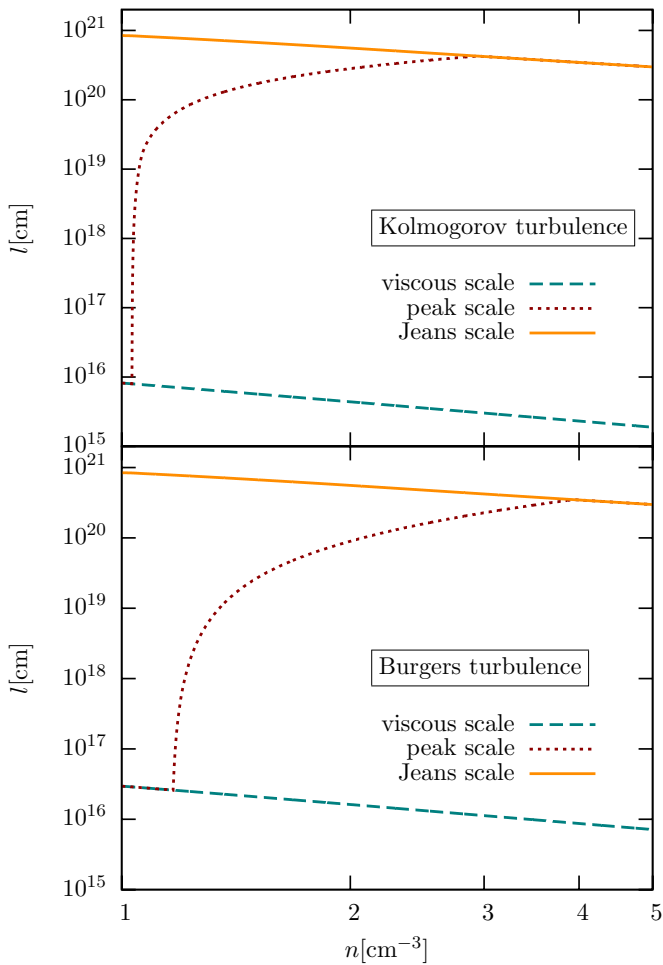
Figure 6. Different characteristic scales as a function of the density. The dashed green line indicates the viscous scale, the dotted red line the scale corresponding to the peak of the magnetic energy spectrum, and the solid orange line the Jeans scale. We show the results for Kolmogorov turbulence in the upper plot and the results for Burgers turbulence in the lower plot.

(A color version of this figure is available in the online journal.)

times (red-colored curve) is a relic of the turbulence spectrum and thus is proportional to ℓ^ϑ.

At each time step we calculate the peak magnetic field strength by solving the stationary case of Equation (20). However, we find that the magnetic field strength exceeds the equipartition field strength on scales larger than the viscous scale. The reason for this is that the ambipolar dissipation rate, which is proportional to B^2/ℓ^2, decreases rapidly in this regime. Thus, it cannot balance the growth rate any longer and we need to set the equipartition field strength as an upper limit $B_{\ell,\max}$. With $B_{\ell,\max}^2/(8\pi) = 1/2\rho v(\ell)^2$ we find the maximum magnetic field strength $B_{\ell,\max} = \sqrt{4\pi\rho}\, v(\ell)$.

Taking the typical turbulent velocity on the scale of the turbulence ℓ to be related to the sound speed by $v(\ell) = (\ell/\ell_J)^\vartheta c_s \simeq (\gamma kT/m)^{1/2}(\ell/\ell_J)^\vartheta$, we find that

$$B_{\ell,\max} = \sqrt{4\pi\gamma kTn}\,(\ell/\ell_J)^\vartheta . \qquad (23)$$

Using the Kazantsev slope, we can extrapolate the magnetic field strength onto the current Jeans length. By this we are able to determine the time evolution of the magnetic field on the Jeans scale.

For this process to be relevant during collapse, the eddy timescale needs to be smaller than the collapse timescale. Thus,
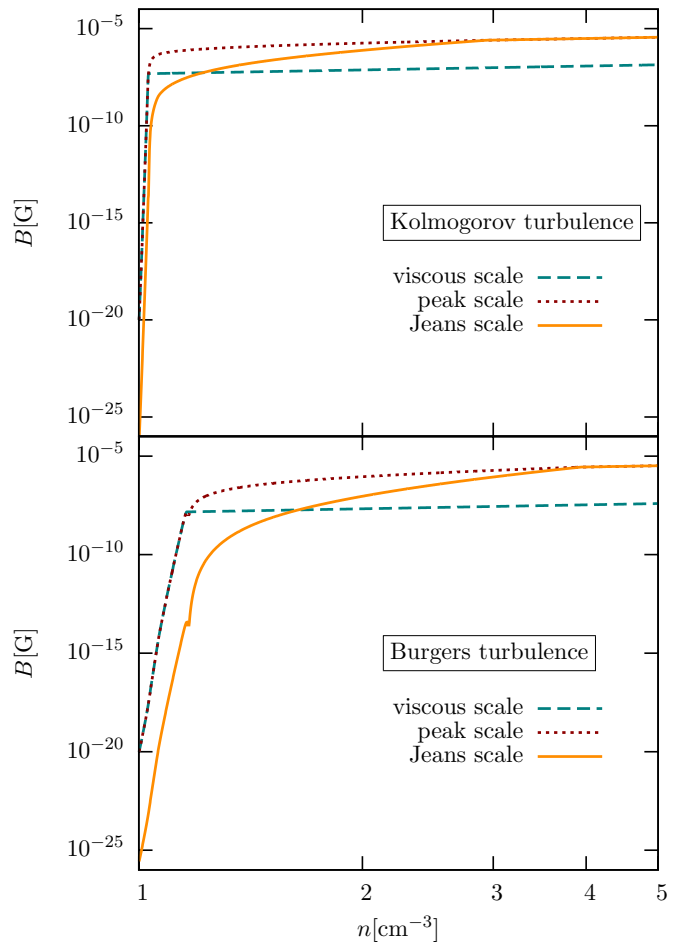
Figure 7. Magnetic field strength as a function of the number density on different scales. The dashed green line corresponds to the field evolution on the viscous scale, the dotted red line to the peak scale, and the solid orange line to the Jeans scale. We show the results for Kolmogorov turbulence in the upper plot and the results for Burgers turbulence in the lower plot.

(A color version of this figure is available in the online journal.)

the small-scale dynamo is unlikely to produce magnetic fields on scales larger than the Jeans scale. Figure 6 shows the viscous, the peak, and the Jeans scale as a function of density. During the small-scale dynamo growth the spectrum of the magnetic energy peaks at the viscous scale. After saturation on the viscous scale the peak moves to larger scales according to Equation (22) until it reaches the Jeans scale.

4.2. Resulting Jeans-scale Magnetic Field

As described in the last section, we determine the magnetic field on the Jeans scale by extrapolation from the peak scale. The result of the large-scale magnetic field is shown in Figure 7 together with the field on the current peak scale and the one on the viscous scale. One can see that the magnetic energy is shifted rapidly onto larger scales. For Kolmogorov turbulence the field on the Jeans scale saturates at a density of roughly 3 cm^{-3} and for Burgers turbulence at a density of roughly 4 cm^{-3}. At the end of dynamo growth on the Jeans scale we have a magnetic field strength of about 10^{-6} G throughout the entire inertial range of the turbulence, i.e., within the Jeans volume.

After the rapid initial dynamo amplification the only way to amplify the magnetic field on the Jeans scale further is gravitational compression, which leads to $B \propto n^{2/3}$. However, the field has already reached equipartition with the kinetic
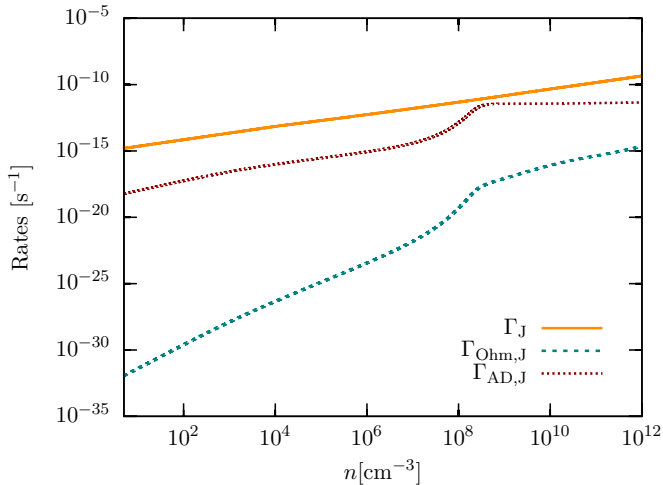
Figure 8. Growth rate on the Jeans scale Γ_J after the dynamo amplification compared to the diffusion rates as a function of the number density. $\Gamma_{Ohm,J}$ and $\Gamma_{AD,J}$ are the Ohmic and ambipolar diffusion rates, respectively.

(A color version of this figure is available in the online journal.)

energy at the end of the dynamo amplification and, thus, increases only with $n^{1/2}$ (see Equation (23)). The growth rate of the magnetic field on the Jeans scale Γ_J is then

$$\Gamma_J = \frac{1}{n}\frac{dn}{dt}. \qquad (24)$$

In Figure 8, we compare the growth rate Γ_J to the ambipolar and Ohmic diffusion rates on the Jeans scale, $\Gamma_{AD,J}$ and $\Gamma_{Ohm,J}$. As Γ_J is always larger than the diffusion rates in the density range shown, the magnetic energy on the Jeans scale is not dissipated again during the collapse. At a density of 10^{12} cm^{-3}, we determine with $B \propto n^{1/2}$ a magnetic field strength of 0.4 G.

4.3. Implications for Numerical Simulations

Our calculations show that, due to the rather small viscosity and resistivity in primordial gas, the hydrodynamical Reynolds number, the magnetic Reynolds number, and the magnetic Prandtl numbers have very high values as long as the magnetic field is not saturated. Such Reynolds numbers are well above what can be reached in numerical simulations, implying that the physical growth rate of the magnetic field largely exceeds the growth rate obtained in numerical simulations. Particularly important here is the fact that the typically unresolved viscous scales are highly relevant for magnetic field amplification even on larger scales. In this sense, numerical simulations can only show the presence of a dynamo, but will typically underestimate the magnetic field amplification rate. This behavior has also been demonstrated in pioneering studies by Sur et al. (2010) and Federrath et al. (2011b).

On the other hand, our results show that magnetic fields quickly saturate once turbulence forms, and the limiting timescale may thus be the timescale on which turbulence is generated. This is again an issue which can be addressed with numerical simulations and, indeed, simulations for instance by Turk et al. (2012) convincingly demonstrated the release of turbulence from the gravitational energy during primordial collapse. Overall, such simulations are thus relevant to explore the origin and generation of turbulence, while the strength of the magnetic field should rather be estimated based on the physical growth rates. As a net effect, we therefore expect that the

magnetic energy is always close to saturation once turbulence is generated in the halo.

5. SUMMARY

We computed the evolution of the magnetic field and its saturation level in typical primordial halos based on the Kazantsev theory of the turbulent dynamo in combination with a detailed description of the physical and chemical processes in zero-metallicity gas. The model is in principle applicable only to magnetic field fluctuations on very small scales. However, when interested in the influence of the field on the overall dynamical evolution of the halo gas, it is most important to understand how saturation occurs on larger scales. To address this problem, we also considered the transport of magnetic energy from the viscous scale to the Jeans scale.

Starting with a weak magnetic seed field of 10^{-20} G, as can be produced by the Biermann battery, we followed the evolution of magnetic field fluctuations on the viscous scale and found that they are amplified very rapidly on timescales much shorter than the free-fall time. As a consequence, the field saturates almost immediately after the onset of gravitational collapse in the halo. By extrapolating the small-scale magnetic field to larger scales and assuming the peak of the magnetic spectrum shifts on the local eddy timescale, we were able to follow the evolution of the magnetic field strength throughout the full inertial range within the Jeans volume. For typical halo parameters, the dynamo growth of the magnetic energy saturates at a density of roughly 3 cm^{-3} for Kolmogorov turbulence and 4 cm^{-3} for Burgers turbulence. At this point in time the field has a strength of about 10^{-6} G. We point out, however, that the field continues to grow in the collapsing gas due to gravitational compression.

Our results show that the magnetic energy on small scales, and more importantly also on dynamically important large scales, can grow to very high values. In order to understand the influence of this strong field on the evolution of the halo gas, it is important to know whether the small-scale magnetic field can be transformed into a coherent large-scale field. One way to produce more coherent magnetic structures is by forming disks, which is suggested by Latif et al. (2011). Moreover, the saturation behavior of the small-scale dynamo should be explored further in the regime Pm < 1, as we have shown that the magnetic Prandtl number is in this regime for high densities.

If indeed the processes discussed here can produce dynamically significant fields on large scales, then the magnetic field will influence the star formation process in high-redshift halos. For example, since recent high-resolution simulations indicate that the accretion disks around the very first stars were strongly susceptible to fragmentation (Turk et al. 2009; Stacy et al. 2010; Clark et al. 2011; Greif et al. 2011; Smith et al. 2011) it is expected that most primordial stars formed as members of binary or higher-order multiple systems with a wide range of masses rather than being isolated, high-mass stars. From studies of low-mass star formation at present day, however, we know that magnetic fields close to the equipartition value can effectively redistribute angular momentum via a process called magnetic braking (Machida et al. 2008b; Mouschovias & Paleologou 1979) and can thereby reduce the fragmentation probability in the disk (Hennebelle & Ciardi 2009; Peters et al. 2011; Hennebelle et al. 2011; Seifried et al. 2011). The correct treatment of magnetic fields in calculations of primordial star formation therefore seems critical to better understand the mass function and multiplicity of metal-free stars.

REFERENCES

Abel, T., Bryan, G. L., & Norman, M. L. 2002, Science, 295, 93
Banerjee, R., & Jedamzik, K. 2004, Phys. Rev. D, 70, 123003
Biermann, L. 1950, Z. Naturfor. Teil A, 5, 65
Boldyrev, S., & Cattaneo, F. 2004, Phys. Rev. Lett., 92, 144501
Bovino, S., Tacconi, M., Gianturco, F. A., & Galli, D. 2011a, A&A, 529, A140
Bovino, S., Tacconi, M., Gianturco, F. A., Galli, D., & Palla, F. 2011b, ApJ, 731, 107
Brandenburg, A., & Subramanian, K. 2005, Phys. Rep., 417, 1
Bromm, V., & Larson, R. B. 2004, ARA&A, 42, 79
Burgers, J. 1948, in Advances in Applied Mechanics, Vol. 1, ed. R. Von Mises & T. Von Kárman (Amsterdam: Elsevier), 171
Choudhuri, A. R. 1998, The Physics of Fluids and Plasmas: An Introduction for Astrophysicists (Cambridge: Cambridge Univ. Press)
Clark, P. C., Glover, S. C. O., Smith, R. J., et al. 2011, Science, 331, 1040
Cyburt, R. H. 2004, Phys. Rev. D, 70, 023505
Elmegreen, B. G., & Burkert, A. 2010, ApJ, 712, 294
Eyink, G. L. 2011, Phys. Rev. E, 83, 056405
Federrath, C., Chabrier, G., Schober, J., et al. 2011a, Phys. Rev. Lett., 107, 114504
Federrath, C., Roman-Duval, J., Klessen, R. S., Schmidt, W., & Mac Low, M.-M. 2010, A&A, 512, A81
Federrath, C., Sur, S., Schleicher, D. R. G., Banerjee, R., & Klessen, R. S. 2011b, ApJ, 731, 62
Glover, S. C. O., & Savin, D. W. 2009, MNRAS, 393, 911
Greif, T. H., Bromm, V., Clark, P. C., et al. 2012, arXiv:1202.5552
Greif, T. H., Johnson, J. L., Klessen, R. S., & Bromm, V. 2008, MNRAS, 387, 1021
Greif, T. H., Springel, V., White, S. D. M., et al. 2011, ApJ, 737, 75
Hennebelle, P., & Ciardi, A. 2009, A&A, 506, L29
Hennebelle, P., Commerçon, B., Joos, M., et al. 2011, A&A, 528, A72
Hennebelle, P., & Teyssier, R. 2007, arXiv:0709.2887
Kazantsev, A. P. 1968, Sov. Phys.—JETP, 26, 1031
Kleeorin, N., & Rogachevskii, I. 2011, arXiv:1112.3926
Klessen, R. S., & Hennebelle, P. 2010, A&A, 520, A17
Kolmogorov, A. 1941, Akad. Nauk SSSR Dokl., 30, 301
Kritsuk, A. G., Norman, M. L., Padoan, P., & Wagner, R. 2007, ApJ, 665, 416
Krumholz, M. R., & McKee, C. F. 2005, ApJ, 630, 250
Kulsrud, R. M., Cen, R., Ostriker, J. P., & Ryu, D. 1997, ApJ, 480, 481
Kulsrud, R. M., & Zweibel, E. G. 2008, Rep. Prog. Phys., 71, 046901
Latif, M. A., Schleicher, D. R. G., & Spaans, M. 2011, A&A, 540, A101
Mac Low, M.-M., & Klessen, R. S. 2004, Rev. Mod. Phys., 76, 125
Machida, M. N. 2010, arXiv:1005.1707
Machida, M. N., Inutsuka, S.-i., & Matsumoto, T. 2008a, ApJ, 676, 1088
Machida, M. N., Matsumoto, T., & Inutsuka, S.-i. 2008b, ApJ, 685, 690
Machida, M. N., Omukai, K., Matsumoto, T., & Inutsuka, S.-i. 2006, ApJ, 647, L1
Machida, M. N., Tomisaka, K., & Matsumoto, T. 2004, MNRAS, 348, L1
Maki, H., & Susa, H. 2004, ApJ, 609, 467
Maki, H., & Susa, H. 2007, PASJ, 59, 787
McKee, C. F., & Ostriker, E. C. 2007, ARA&A, 45, 565
Mouschovias, T. C., & Paleologou, E. V. 1979, ApJ, 230, 204
Peters, T., Banerjee, R., Klessen, R. S., & Mac Low, M.-M. 2011, ApJ, 729, 72
Pinto, C., & Galli, D. 2008, A&A, 484, 17
Pinto, C., Galli, D., & Bacciotti, F. 2008, A&A, 484, 1
Price, D. J., & Bate, M. R. 2007, Ap&SS, 311, 75
Rogachevskii, I., & Kleeorin, N. 1997, Phys. Rev. E, 56, 417
Schekochihin, A. A., Boldyrev, S. A., & Kulsrud, R. M. 2002a, ApJ, 567, 828
Schekochihin, A. A., Cowley, S. C., Hammett, G. W., Maron, J. L., & McWilliams, J. C. 2002b, New J. Phys., 4, 84
Schekochihin, A. A., Haugen, N. E. L., Brandenburg, A., et al. 2005, ApJ, 625, L115
Schekochihin, A. A., Iskakov, A. B., Cowley, S. C., et al. 2007, New J. Phys., 9, 300
Schleicher, D. R. G., Banerjee, R., Sur, S., et al. 2010, A&A, 522, A115
Schleicher, D. R. G., Galli, D., Glover, S. C. O., et al. 2009, ApJ, 703, 1096
Schmidt, W., Federrath, C., & Klessen, R. 2008, Phys. Rev. Lett., 101, 194505
Schober, J., Schleicher, D., Federrath, C., Klessen, R., & Banerjee, R. 2012, Phys. Rev. E, 85, 026303
Seifried, D., Banerjee, R., Klessen, R. S., Duffin, D., & Pudritz, R. E. 2011, MNRAS, 417, 1054
Sigl, G., Olinto, A. V., & Jedamzik, K. 1997, Phys. Rev. D, 55, 4582
Silk, J., & Langer, M. 2006, MNRAS, 371, 444
Smith, R. J., Glover, S. C. O., Clark, P. C., Greif, T., & Klessen, R. S. 2011, MNRAS, 414, 3633
Stacy, A., Greif, T. H., & Bromm, V. 2010, MNRAS, 403, 45
Subramanian, K. 1997, arXiv:astro-ph/9708216
Sur, S., Federrath, C., Schleicher, D., Banerjee, R., & Klessen, R. S. 2012, MNRAS, in press (arXiv:1202.3206)
Sur, S., Schleicher, D. R. G., Banerjee, R., Federrath, C., & Klessen, R. S. 2010, ApJ, 721, L134
Tan, J. C., & Blackman, E. G. 2004, ApJ, 603, 401
Turk, M. J., Abel, T., & O'Shea, B. 2009, Science, 325, 601
Turk, M. J., Oishi, J. S., Abel, T., & Bryan, G. L. 2012, ApJ, 745, 154
Turner, M. S., & Widrow, L. M. 1988, Phys. Rev. D, 37, 2743
Vazquez-Semadeni, E., Canto, J., & Lizano, S. 1998, ApJ, 492, 596
Wardle, M., & Ng, C. 1999, MNRAS, 303, 239
Wise, J. H., & Abel, T. 2007, ApJ, 665, 899
Xu, H., Li, H., Collins, D. C., Li, S., & Norman, M. L. 2011, ApJ, 739, 77
Xu, H., O'Shea, B. W., Collins, D. C., et al. 2008, ApJ, 688, L57